Cellulose (2018) 25:735–751
https://doi.org/10.1007/s10570-017-1598-x

ORIGINAL PAPER

Preparation of magnetic $MnFe_2O_4$-Cellulose aerogel composite and its kinetics and thermodynamics of Cu(II) adsorption

Sheng Cui · Xue Wang · Xin Zhang · Wei Xia · Xianglong Tang · Benlan Lin · Qi Wu · Xin Zhang · Xiaodong Shen

Received: 31 July 2017 / Accepted: 27 November 2017 / Published online: 6 December 2017

Abstract In this paper, a $MnFe_2O_4$-Cellulose magnetic composite aerogel (MnCA) with high adsorption capacity was fabricated by in situ incorporating $MnFe_2O_4$ to regenerated cellulose hydrogel matrix, followed by CO_2 supercritical drying. A green synthetic strategy was performed by using renewable cellulose materials, environmentally benign cellulose solvents and facile synthetic conditions. The results showed that the obtained magnetic cellulose aerogel had a continuous and tiered three dimensional network with interconnected fibrils of about 30 nm in width, which was similar to those of cellulose aerogel prepared from NaOH/urea solution via CO_2 supercritical drying. Meanwhile, they had high specific surface areas of 236–288 m^2/g and total pore volume of 0.55–0.88 cm^3/g. In addition, the hybrid aerogel showed superparamagnetism with maximum saturation magnetization reaching up to 18.53 emu/g. The magnetic nanocomposite aerogel could be used for biological and environmental applications. The adsorption test showed that MnCA had rapid adsorption rate and excellent adsorption ability of removing heavy metal ions in aqueous solution which could attain to 63.3 mg/g within 100 min. Moreover, all the composite aerogels exhibited good reusability and could be easily reused from the water after adsorption.

Keywords Magnetic aerogel · $MnFe_2O_4$-Cellulose · Composites · Copper ion · Adsorption

S. Cui (✉) · X. Wang · X. Zhang · X. Tang · B. Lin · X. Shen
State Key Laboratory of Materials-Oriented Chemical Engineering, College of Materials Science and Engineering, Nanjing Tech University, Nanjing 210009, China
e-mail: cui2002sheng@126.com

W. Xia (✉)
Division for Applied Materials Science, Department of Engineering Sciences, Uppsala University, 75121 Uppsala, Sweden
e-mail: Wei.Xia@angstrom.uu.se

Q. Wu · X. Zhang
Department of Neurosurgery, Nanjing General Hospital, Nanjing 210002, China

S. Cui · X. Wang · X. Zhang · X. Shen
Jiangsu Collaborative Innovation Center for Advanced Inorganic Function Composites, Nanjing 210009, China

Introduction

There is a growing worldwide concern of the urgent need to control the issue of environmental pollution from the growth of population and development of industries. The treatment of sewage, containing heavy metals, has become hot issue due to various heavy metal ions have been more often found in waters (Shen et al. 2015). The sources of effluents are immoderately discharged from industries directly or indirectly, such as metallurgy (Qarri et al. 2015), chemical

manufacturing (Baccar et al. 2009), electroplating (Liu et al. 2014; Wu et al. 2015), mining operations (Pizarro et al. 2015; Shen et al. 2015), etc. The increasing level of heavy metals in environment brings a serious threat to human health, living resources and ecological systems. For example, Cu(II) is toxic to aquatic organism even at very low concentration in natural waters. Unlike organic contaminants, heavy metals are non-biodegradable and tend to accumulate in living organisms. For example, when the intake of copper by human beings is excessive, it may cause the damage of hepatic, renal, capillary and central nervous problems (Shen et al. 2015; Zeng et al. 2015).

Nowadays heavy metals are the environmental priority pollutants, and their contamination is becoming one of the most serious environmental problems. Therefore, several treatment techniques have been developed for the removal of toxic metals from aqueous solution including chemical precipitation, ion-exchange, adsorption, membrane filtration, coagulation flocculation, flotation and electrochemical method (Fu and Wang 2011). Among of the techniques used for the sewage treatments, adsorption is now recognized as an effective, flexible and economical method for heavy metal wastewater treatment (Fu and Wang 2011). Because of its low adsorption temperature, selectivity, purification, and the simple operation process. Ferrite has been widely studied for heavy metal wastewater treatment (Kefeni et al. 2017; Naushad et al. 2017), by adding iron to wastewater and controlling process condition, then the heavy metal ions in wastewater enter into ferrite lattice and form composite ferrite under the action of inclusion and entrainment of ferrite, and then by means of solid liquid separation, removal of heavy metals in wastewater. However, the adsorption capacity of this method is not high (Ren et al. 2012b). In addition, the ferrite coprecipitation needs a certain temperature, and it needs to be carried out under oxygen condition with a high operation cost and it is difficult to operate continuously, causing long processing time and the sediment is difficult to separate(Rajput et al. 2016). Activated carbon (AC) based adsorbents are widely used for the removal of heavy metals. ACs' large micropore and mesopore volumes and high surface area help the removal. A large number of researchers are studying the use of AC for removing heavy metals in the past few years (Jusoh et al. 2007; Kang et al. 2008; Monser and Adhoum 2002). One of the most disadvantages of AC is the high recycling expensed to the limited adsorption capacity and poor regeneration property in the practical application. It is obvious that the regeneration of saturated adsorbents is a critical factor that should be considered in the adsorbent selection process (Dou et al. 2011). Besides, when it is used under various operational conditions, activated carbon frequently encounters such problems, e.x. secondary pollution, pore clogging, oxidative degradation, corrosion, hygroscopicity, lower selectivity and limited modification flexibility (Dou et al. 2011; Liu et al. 2009; Shim et al. 2006). Therefore, it's very necessary to seek for a new effective adsorbent with high adsorption capacity, high specific surface areas, abundant micropores, easily recovered regeneration, abundant and inexpensive sources. In recent years, aerogels are regarded as one of the promising high performance insulation for building application (Baetens et al. 2011), meanwhile, high porosity and large specific surface area showed superior adsorption ability, is good performance of the adsorbent, which can be widely applied in wastewater treatment, air purification and nuclear waste disposal, and other areas of the environmental protection (Abramian and El-Rassy 2009; Cui et al. 2011; Mi et al. 2012; Standeker et al. 2007).

Cellulose aerogel (Cai et al. 2008; Wang et al. 2012) is getting an increasing interest as a class of nature biodegradable functional material. Cellulose aerogel possesses high surface area, high porosity and extremely low density similar to SiO_2 aerogel (Lin et al. 2013), and has some unique properties such as renewability, easy degradability and biocompatibility, which make it valuable in the field of heat insulation, adsorption, catalysis, electricity and magnetism, biomaterial and pharmaceutical, etc. (Maleki 2016; Mu et al. 2016; Stergar and Maver 2016). Cellulose aerogel consists of cross-linked three-dimensional (3D) architectures formed by self-assembly of cellulose chains as a result of hydrogen-bond interaction, and has been considered as a class of ideal green matrix materials to encapsulate functional materials (Cai et al. 2012; Liu et al. 2012b; Olsson et al. 2010). Besides, the interior pore structure of cellulose aerogel makes it appropriately used as reaction sites that could provide micro/nanoscale confined spaces for hosting nanoparticles (Liu et al. 2012b; Olsson et al. 2010). $MnFe_2O_4$ nanoparticle, as one of the most important inverse spinel type of iron oxides, exhibits unique performances such as photo adsorption, electrical

conductivity and magnetic responsiveness (Aslibeiki et al. 2016; Zeng et al. 2004). Meanwhile, Due to its small particle size effect, good biocompatibility, nontoxicity, excellent chemical and thermal stability, favorable hysterical properties, $MnFe_2O_4$ has been widely used as magnetic targeting drug carriers, MRI contrast agents, adsorbents for water purification, catalytic materials etc.

It could be a potential way of preparation of a new adsorbent via combining cellulose aerogel and magnetic nanomaterials. Duo to the high surface area and high porosity, cellulose gel could be used as an ideal template which can be used to fabricate nanomaterial and prevent the aggregation of magnetite. Therefore, a facile approach based on the chemical precipitation using cellulose aerogel as a template was studied to synthesize a magnetic $MnFe_2O_4$-Cellulose aerogel composite adsorbent (Liu et al. 2011, 2012a). A green low-cost LiOH/urea aqueous solution was carried out to fabricate cellulose hydrogels (Cai and Zhang 2006), and the microcrystalline cellulose was used as the cellulose source. The nanoparticle size, pore parameters, magnetic properties, and mechanical properties of the synthetic $MnFe_2O_4$-Cellulose aerogels could be tailored by adjusting the concentrations of the initial reactants. As an example of potential applications, this $MnFe_2O_4$-Cellulose aerogel nanocomposite was used as an environmentally friendly adsorbent for the removal of heavy metals in the wastewater treatment. Through adsorption kinetic and adsorption thermodynamics, its maximum adsorption abilities were systematically investigated. Meanwhile, The separation and reusability of magnetic aerogel were also investigated in this work.

Experimental Section

Materials

Microcrystalline cellulose (MCC) with the degree of polymerization (DP) ~ 200–300 was bought from Sinoreagent Chemical Reagent Co., Ltd. Lithium hydroxide (LiOH), urea, Citric acidferric chloride ($FeCl_3$ $6H_2O$), manganous chloride ($MnCl_2{\cdot}4H_2O$) were purchased from Shanghai Aladdin Chemical Reagent Co., Ltd. Copper chloride ($CuCl_2$) was obtained from Shanghai chemical reagent Co., Ltd. Sodium diethyldithiocarbamate (DDTC) was purchased from Jinshan New Chemical Reagent Factory in Shanghai. Ethylenediaminetetraacetic acid disodium salt (Na_2-EDTA), Carbon tetrachloride (CCl_4) and Ammonium chloride (NH_4Cl) were purchased from Sinoreagent Chemical Reagent Co., Ltd. All chemicals used were either AR or GR-grade.

Preparation of magnetic $MnFe_2O_4$-Cellulose aerogel

The dried microcrystalline cellulose (3.0 g) was mixed with 4.6% of the alkali aqueous solution of LiOH/Urea/H_2O (4.6 wt %/15 wt %/80.4 w %) under magnetic stirring for 30 min. Then the cellulose solution was transferred to a refrigerator and frozen at – 15 °C for 12 h. The frozen cake was taken out and vigorously stirred for 5 min at ambient temperature to obtain a transparent cellulose solution. The cellulose solution was centrifuged at 9000 rpm for 3 min to remove air bubbles. The resulting solution was cast on a plastics mold, and immersed into the methanol coagulation bath for regeneration. The regenerated cellulose hydrogel was washed with excess deionized water to remove the chemical residues. After removal of excess impurities, the cellulose hydrogels were immersed in a freshly prepared aqueous solution of $FeCl_3$ and $MnCl_2$ (100 ml) with a constant mole ratio of $[Fe^{3+}]/[Mn^{2+}] = 2$, and the mixture was held at temperature of 25 °C for 24 h. After that, the hydrogel including Fe^{3+}/Mn^{2+} metal ion solution was placed in reactor containing 50 mL of NaOH solution (2 mol/L). The color of the sample changed immediately from orange/green to blak as inorganic nanoparticles were formed in the hydrogel matrix. There after, the reaction was subsequently heated to 90 °C and kept for 5 h. Finally, the resulting sample was washed thoroughly with excess deionized water to remove chemical residues. The absorbed water in the $MnFe_2O_4$-cellulose hydrogel was exchanged with ethanol (EtOH), which was then exchanged with the final drying liquid. Drying with supercritical CO_2 was performed using a supercritical CO_2 fluid extraction HELIX 1.1, Applied Separations Inc., by exchanging ethanol to liquid CO_2 at 10 MPa for 8 h at 50 °C, and finally by slow release CO_2 at 40 °C. Pure cellulose aerogel was prepared by the same method as contrast and coded as CA. By changing the molarity of $MnCl_2$ solution from 0.01 mol/L to 0.10 mol/L, three samples of magnetic $MnFe_2O_4$-Cellulose aerogel were prepared and coded as MnCA-001, MnCA-005 and MnCA-010 respectively.

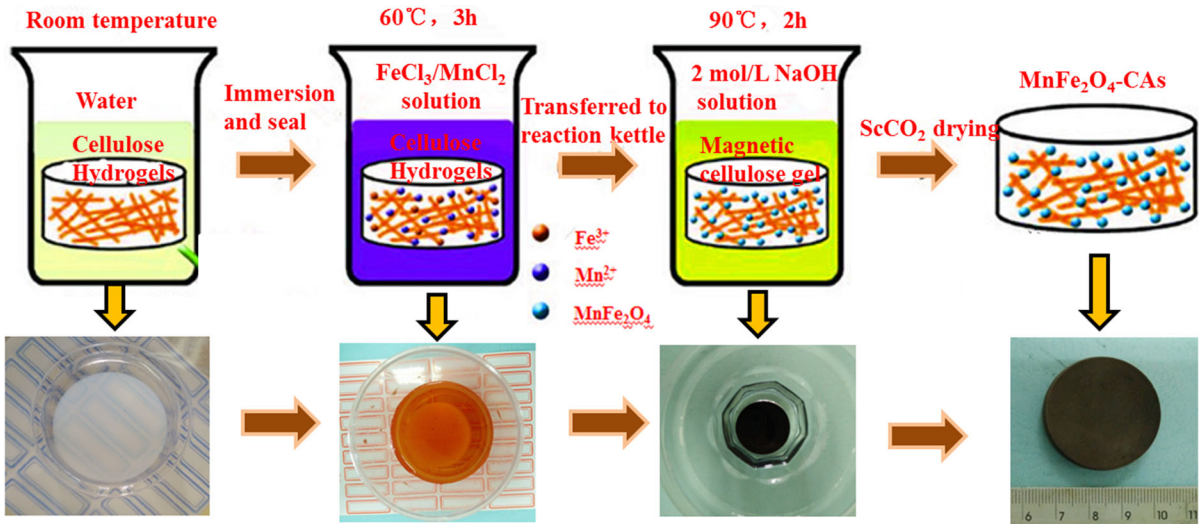

Fig. 1 Schematic illustration for the preparation of magnetic cellulose composite aerogel

Characterization and test method

$MnFe_2O_4$-cellulose aerogels were characterized by X-ray diffraction (XRD), X-ray photoelectron spectroscopy(XPS), Fourier transform infrared spectra (FT-IR), Scanning electron microscopy (SEM), transmission electron microscope (TEM), Thermal gravimetric analysis (TGA) and N_2 adsorption–desorption measurement etc. XRD patterns were obtained using a Rigaku Smart Lab 3000 (CuKα (target) radiation ($\lambda = 1.5418$ Å)) with a scan rate (2θ) of 4°/min and a scan range from 10° to 80°. XPS was carried out using a Thermo Escalab 250Xi XPS spectrometer equipped with a dual X-raysource using Al Kα. FTIR was implemented by a Nicolet Nexus 670 FTIR instrument in the range from 400 to 4000 cm^{-1} with the a resolution 4 cm^{-1}. TGA was performed by NETZSCH STA449C Thermogravimetric analyzer from 30 °C to 1000 °C with a heating rate of 10 °C/min under argon atmosphere. The magnetization curves of nanoparticles were measured using a magnetometer (Zhengxian HH-15) at the room temperature under circulating magnetic field between − 5000 and 5000 Oe at 298 k. SEM was conducted using a LEO-1530VP field emission scanning electron microscope operating at 6 kV. Microstructure of the aerogels were analyzed using TEM (JEOL JEM-2100 (UHR)) operating at the acceleration voltage of 200 kV. Surface areas, pore volume and pore distribution were measured by nitrogen adsorption/desorption porosimetry by using an APPLICATION V-Sorb 2800P surface area and pore distribution analyser. Samples were degassed in a vacuum at 100 °C for 6 h.

Adsorption of Cu(II) on $MnFe_2O_4$-cellulose aerogel

Solutions with different concentrations of Cu(II) were prepared using $CuCl_2{\cdot}H_2O$ as the source of heavy metal ions and sodium diethyldithiocarbamate (DDTC) as color developing agent, respectively. The pH value was adjusted to 4 using HCl (0.1 mol/L). The as-prepared CA and MnCA were used as adsorbents. For the adsorption kinetic study, 0.1 g of adsorbent was added to 50 mL solutions with a Cu(II) initial concentration of 10 ug/mL. After a specified time, the adsorbent was separated by centrifugation from the Cu(II) solutions, and the supernatant was collected and analyzed using aultra violet spectrophotometer at 440 nm to measure the concentration of Cu(II) in there maining solution. For the adsorption isothermal study, 50 mg of adsorbent was added to 25 mL of solution with different concentrations under oscillation for 2 h at 40 °C. After the centrifugal separation, according to tested the absorbance value of Cu(II) in the supernatant, the Cu(II) concentration of remaining solution, adsorption capacity and removal efficiency could be calculated by Eqs. (1), (3)and (4).

$$A = 0.0192C + 0.0123 \quad (1)$$

$$C_e = \frac{C}{100V_1} \quad (2)$$

$$Q_e = \left(\frac{(C_0 - C_e) \times V_2}{m_1}\right) \quad (3)$$

$$S(\%) = \frac{C_0 - C_e}{C_0} \times 100\% \quad (4)$$

where C (ug) is means to the Cu(II) content of remaining solution and could be calculated via different absorbance value. V_1 is the supernatant volume (mL) and C_e is the Cu(II) concentration of remaining solution (mg/mL) and Q_e is the amount of Cu(II) adsorbed perunit weight of the adsorbent at equilibrium (mg/g), V_2 is volume (mL) of adding initial Cu(II) solution, S is the Cu(II) removal efficiency (Fig. 1).

Results and discussion

XRD analysis was carried out for clarifying the crystal phases and phase compositions of the synthesized $MnFe_2O_4$ particles. The XRD results of pure cellulose aerogel (PCA) and magnetic $MnFe_2O_4$-Cellulose aerogel (MnCA) with different $MnFe_2O_4$ content were shown in Fig. 2, which shows there are two phases. The specific cellulose peaks can be found at around 12.3°, 20.2°, and 22.0° for both PCA and MnCA, corresponding to (1–10), (110) and (020) planes of cellulose II type. Zhang et al. previously reported that the structure of cellulose changed from type I to type II in the alkali urea solution (Cai et al. 2008; Dassanayake et al. 2016). The peaks of MnCA at around 29.7°, 35.2°, 42.6°, 52.8°, 56.2°, 61.7°and 73.2°are consistent with the JCPDS file of Jacobsite $MnFe_2O_4$ (Vernekar et al. 2015) (No. 10-10319). The crystallization degree of cellulose II gradually reduced and the crystallization degree of manganese ferrite gradually increased with the increase of $MnFe_2O_4$ content, indicating the formation of $MnFe_2O_4$ with an inverse spinel crystalline structure (Fig. 3).

In order to verify the oxidation state of the synthesized $MnFe_2O_4$ particle precisely, the XPS spectrum result revealed that the Fe 2p peaks at the binding energies of 710.80 and 725.20 eV, closely correspond to the Fe $2p_{3/2}$ and Fe $2p_{1/2}$ spin–orbit peaks of $MnFe_2O_4$ (Wang et al. 2016). The Mn 2p

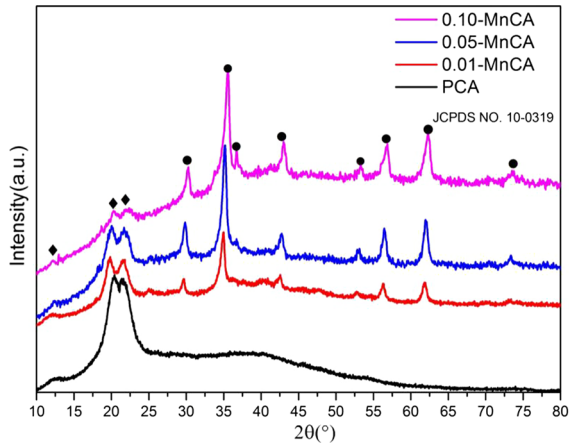

Fig. 2 XRD patterns of PCA and different $MnFe_2O_4$ content MnCA, respectively

peaks at the binding energies of 640.84 and 652.56 eV, closely correspond to the Mn $2p_{3/2}$ and Mn $2p_{1/2}$ spin–orbit peaks. The satellite peaks at around 530.85 and 533.25 eV correspond to the O 1 s. Through the calculation of peak are as S_{Fe}/S_{Mn} is 1.972 in manganese iron. It closely corresponds to the Fe/Mn atomic ratio in $MnFe_2O_4$.

Micro/nanoscale 3D structure of the aerogels allows guest molecules to penetrate into their inner spaces (Fig. 4a, b, c). Meanwhile, strong electrostatic interactions between Mn^{2+}/Fe^{3+} ions and cellulose macromolecules, on account that the electron-rich oxygen atoms of polar hydroxyl and ether groups in cellulose would result in the immobilization of cations in the aerogels matrix. The TEM images of MnCA reveal the presence of $MnFe_2O_4$ in cellulose matrix (Fig. 4). The HRTEM image (Fig. 4e) show the lattice spaceis approximate 0.245 nm which corresponds to the lattice space along (222). The corresponding SAED pattern exhibits typical ring patterns of nanocrystalline materials, and is consistent with the lattice spacing of inverse spinel cubic $MnFe_2O_4$, shown in Fig. 4f.

The scanning electron microscopy of the composite aerogel prepared at the concentrations of the cellulose aerogels and the different initial iron-manganese salts is shown in Fig. 5. The prepared magnetic composite fibers, like the prepared pure cellulose aerogels. The aerogels still retain the inherent three-dimensional porous network structure of the cellulose aerogels, and the magnetic ferrite particles are formed in the pores of the cellulose fibers and are compared with the internal

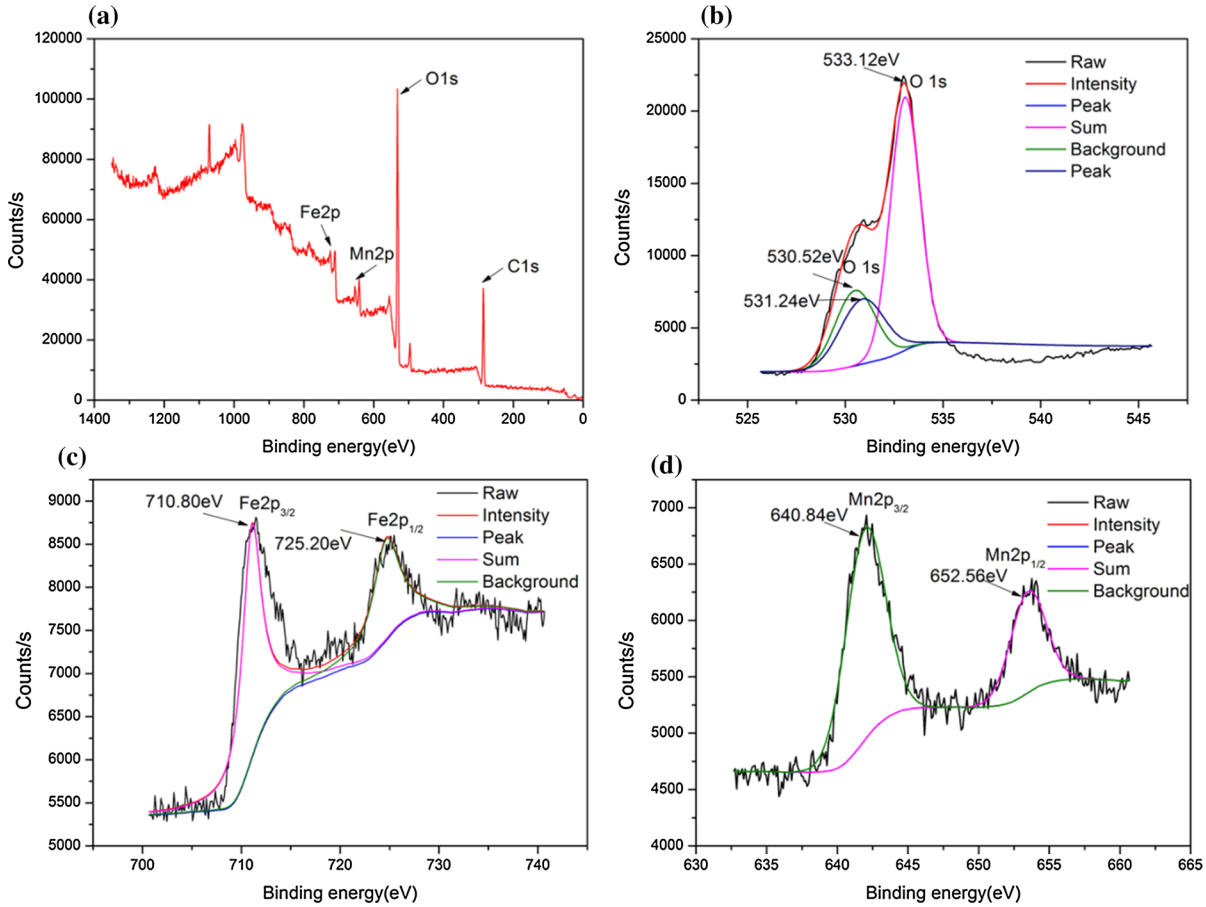

Fig. 3 **a** XPS spectrum of $MnFe_2O_4$-Cellulose Aerogel, **b** O 1 s spin–orbit peaks, **c** Fe 2p spin–orbit peaks, **d** Mn 2p spin–orbit peaks

structure of the pure cellulose aerogels. The magnetic nanoparticles make the three-dimensional space network of magnetic cellulose aerogels look more robust and more uniform in the distribution of the pore structure. The formation of a small amount of magnetic ferrite nanoparticles in the three-dimensional network structure of cellulose also causes the microstructure of the magnetic aerogels to change (as shown in (c) and (d) in Fig. 5). In the reaction process of magnetic cellulose aerogels, the microfreater of $MnFe_2O_4$ was prepared by coprecipitation of the pore structure of cellulose wet gel, and the growth of inorganic nanometer ions was adjusted by adjusting the initial concentration of $FeCl_3/MnCl_2$ salt solution. At the same time, the porous network structure of the cellulose wet gel can also be able to continuously immerse the iron-manganese precursor solution on the one hand so that the magnetic ferrite cellulose composite aerogel can continue to maintain the three-dimensional porous network structure of cellulose fibers, But also to ensure that the formation of magnetic nano-ions can be more uniform distribution.

The FTIR spectra of MnCA present two new peaks located at 631 and 546 cm^{-1} (see Fig. 6). The band at 3039–3710 cm^{-1} assigns to the stretching vibrations of hydroxyl groups. The peak located at 3444 cm^{-1} of MnCA is close to the peak of cellulose at 3443 cm^{-1}. Cellulose is rich in hydroxyl group in different adjacent carbon, but the synthesis of $MnFe_2O_4$ didn't influence hydroxyl group.

N_2 adsorption–desorption isotherms provide useful information of the pore structures of MnCAs (see Fig. 7). All isotherms could be classified to type IV according to IUPAC classification, and the adsorption–desorption loops are the type H3, which reveals the existence of slit-shaped pores. The adsorption uptakes in the P/P_0 range between 0 and 0.6 increases slightly for all samples, indicating the existence of a

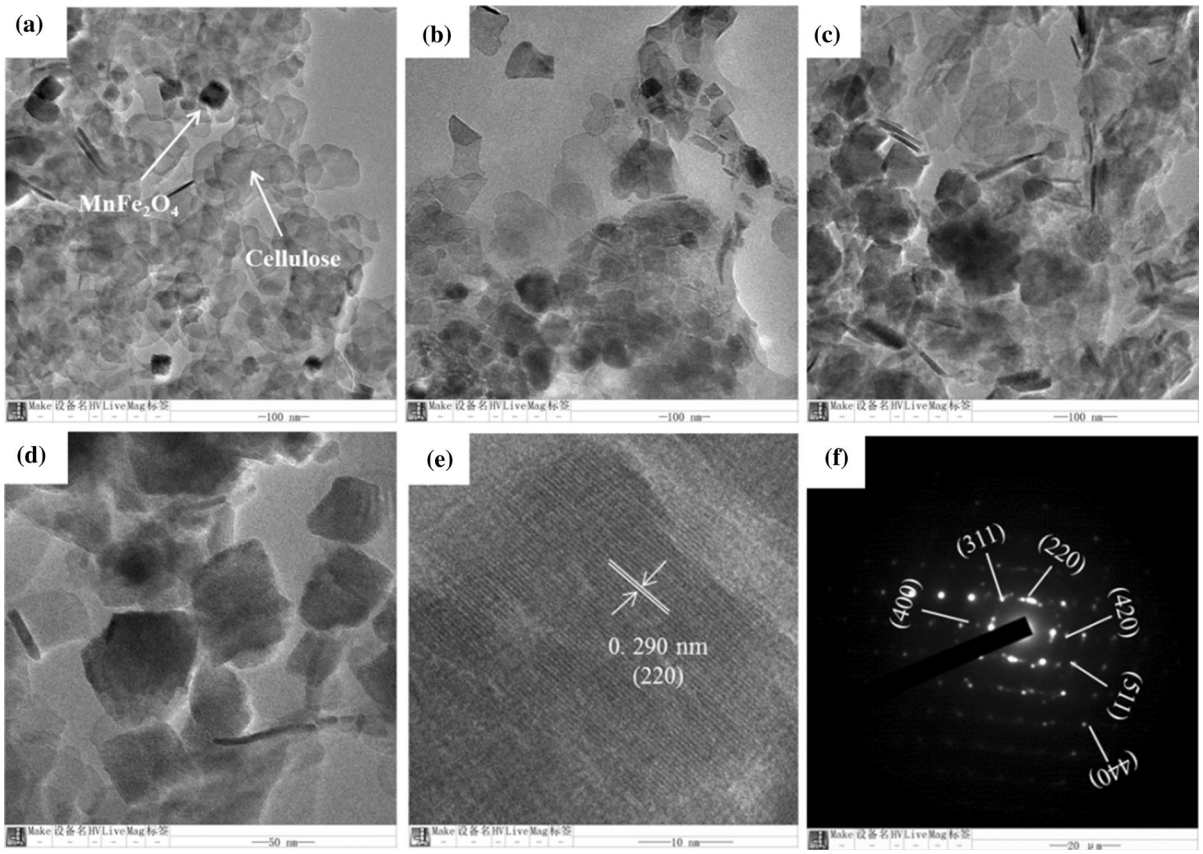

Fig. 4 TEM images of magnetic cellulose aerogels, **a** MnCA-001, **b** MnCA-005, **c**, **d** MnCA-010, **e** HRTEM images of MnCA-001, **f** SAED pattern of MnCA-001

few of micropores. Meanwhile, nitrogen molecules are gradually adsorbed on the internal surface of pores from single to multilayer in this period. Thereafter, the adsorption amounts increase in the range of 0.6–0.99, which generates obvious hysteresis loops, and still does not reach a plateau near the P/P_0 of 0.99, revealing the presence of mesopores and macropores. The results are in good agreement with the observation from SEM images.

BET and BJH analyses show the specific surface areas and pore volumes of 229 m^2/g and 0.67 cm^3/g for CA, 236 m^2/g and 0.5524 cm^3/g for MnCA-0.01, 256 m^2/g and 0.77 cm^3/g for MnCA-0.05, and 288 m^2/g and 0.88 cm^3/g for MnCA-0.10, respectively, as shown in Table 1. It could be seen that the insertion of $MnFe_2O_4$ improves the nanopore characteristic parameters of the composites compared with those of PCA. The specific surface area and pore volume of the composites are affected by the content of incorporated $MnFe_2O_4$ nanoparticles.The specific surface area of MnCA apparently increase with the increasing of the $MnFe_2O_4$ nanoparticles content. These enhancement phenomena could be on account that the insertion of higher content of nanoparticles more effectively strengthens the 3D skeleton structure of the aerogels, leading to more resistant to shrinkage and collapse during the drying treatment.

Taking into account the thermal stability of the material in the application process, so compared the cellulose aerogels and magnetic cellulose aerogels thermogravimetric curve, from Fig. 8 can be seen, magnetic ferrite. The thermogravimetric curve of MnCA is consistent with the thermal degradation trend of cellulose aerogel and same obvious mass loss occurs mainly in three stages. The first stage is about 40–120 °C. The first stage weight loss is caused by the prepared gas. The gel adsorbs a small amount of water, because the surface of the cellulose aerogels is rich in

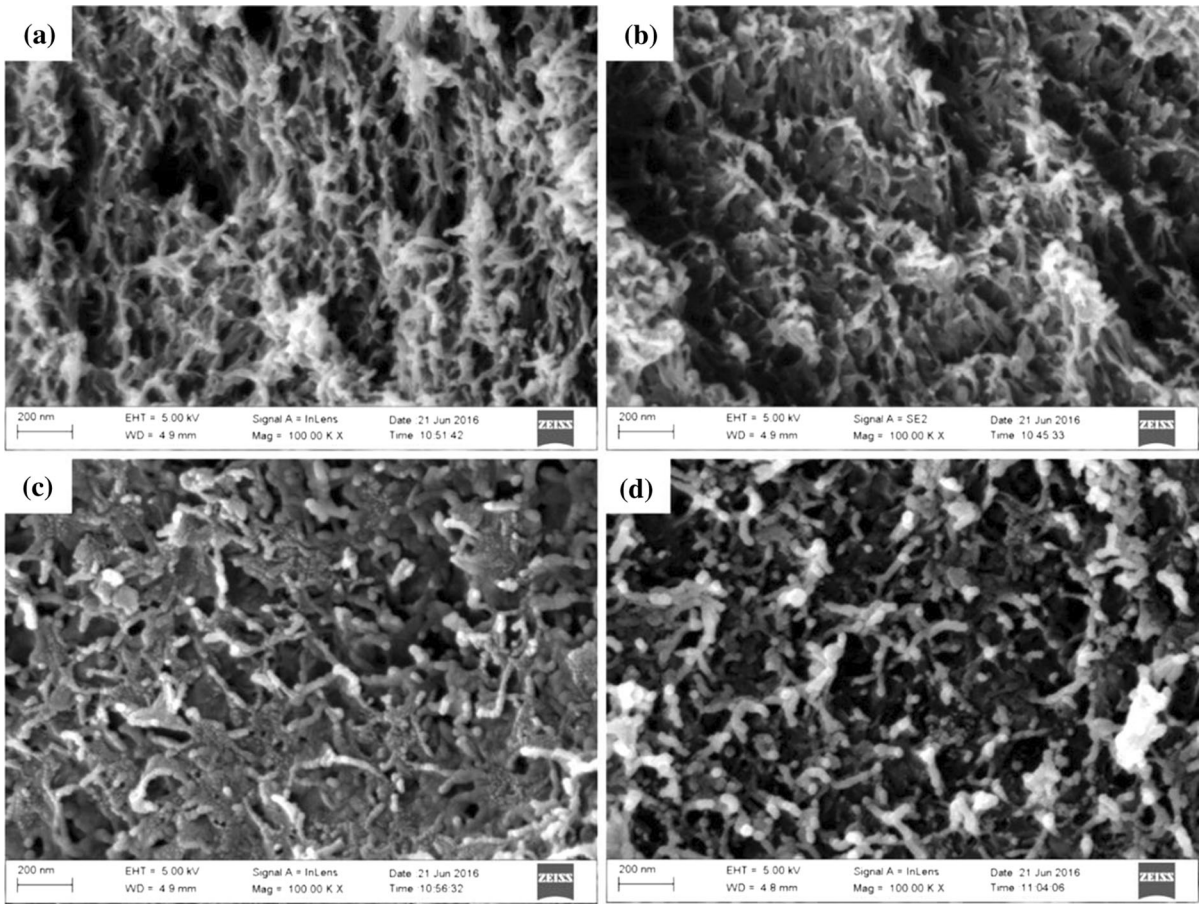

Fig. 5 SEM images of cellulose aerogel and magnetic cellulose aerogels, **a**–**d** were for PCA, MnCA-001, MnCA-005 and MnCA-010, respectively

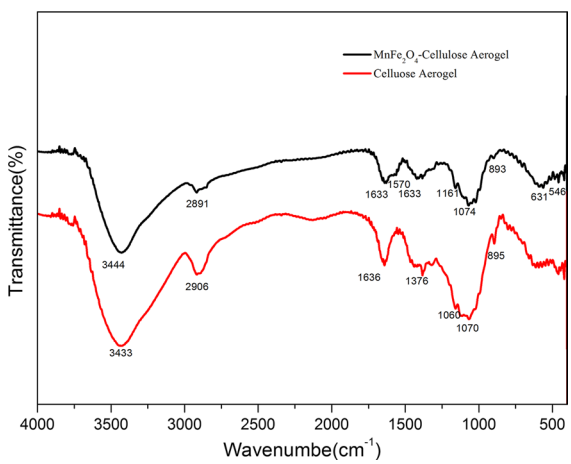

Fig. 6 FTIR spectra of MnCA and PCA, respectively

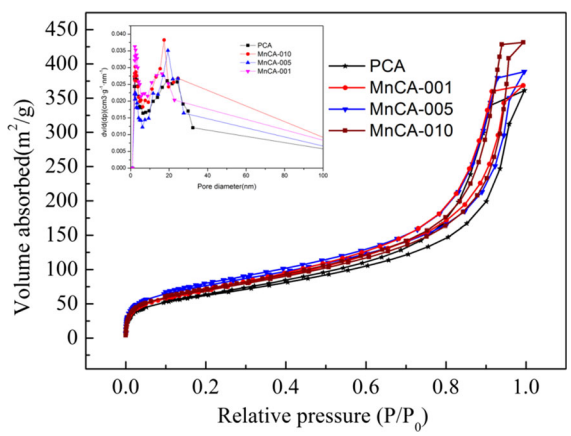

Fig. 7 N_2 Adsorption–desorption isotherms and pore size distributions of CA, MCA-0.01, MCA-0.05, MCA-0.10

Table 1 Physical property parameters of CA and MnCA-0.01, MnCA-0.05 and MnCA-0.10

Sample	$MnFe_2O_4$ (wt %)	Density (mg/cm^3)	S_{BET} (m^2/g)	Pore size (nm)	Pore volume (cm^3/g)	Porosity (%)	Satuation magnetization (emu/g)
CA	/	0.1021	229	13.33	0.6734	82.6	/
MnCA-001	14.1	0.1245	236	11.70	0.5524	78.2	1.934
MnCA-005	26.2	0.1829	256	12.33	0.7733	65.4	9.152
MnCA-010	34.1	0.2087	288	13.99	0.8805	52.6	18.534

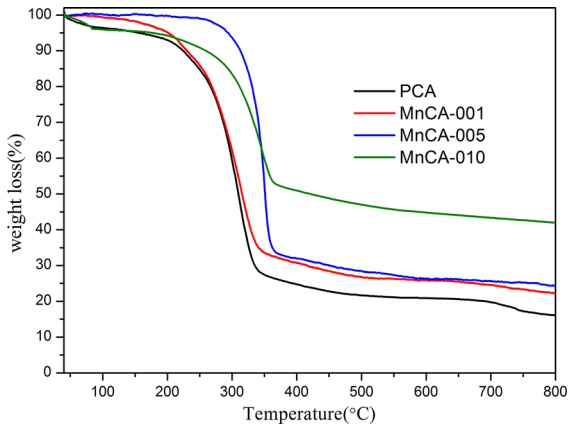

Fig. 8 The TG Curves of CA and MnCA-001, MnCA-005, MnCA-010

hydroxyl, easy to adsorb the air in the water, with the temperature rise, the adsorption of water in the cellulose will be volatile. The second stage is about 120–350 °C, can also be subdivided into two stages, 200 °C before the weight loss can be considered cellulose disaggregation and "vitrification" transformation, 200 °C after the apparent weight loss is mainly cellulose Pyrolysis, converted into gas escape. The third stage starts at about 350 °C, and the residual carbon and ash are decomposed into charcoal and the organic functional groups on the surface of manganese ferrite. The residual sample is stabilized at 750 °C, indicating that the magnetic cellulose Gel in the low temperature range has good stability, to meet the general needs of the environment, magnetic cellulose aerogels compared to cellulose aerogels thermal stability has increased. At the same time, with the increase of the concentration of Fe–Mn salt precursor, the thermal stability of the Fe–Mn salt solution is also increased due to the increase of the precursor solution concentration, which makes the Fe–Mn salt solution further disperse and balance in the three-dimensional network structure of cellulose fiber of the $MnFe_2O_4$ in the cellulose substrate distribution is more uniform, enhance the overall thermal stability of the material.

The room-temperature hysteresis cycles of the MnCA nanocomposites show the absence of hysteresis and coercivity (Fig. 9a, b), which is the characteristic of superparamagnetic behavior caused by the particle size of $MnFe_2O_4$ smaller than the related critical single-domain size. All curves increase rapidly with increasing applied magnetic field. The saturation magnetization (Ms) values are 1.934 emu/g for MnCA-0.01, 9.152 emu/g for MnCA-0.05, and 18.534 for MnCA-0.10, respectively. Apparently, the Ms values significantly increased as the total concentration of the $FeCl_3/MnCl_2$ salts increased, which shows the tailorability of the magnetic property. Additionally, considering the nanoparticles contents in the samples (14.1, 26.2, and 34.1%), the corresponding calculated Ms values are 11.3, 37.8, and 52.8 emu/g, which are smaller than the half of the theoretical Ms of 19.846 emu/g for 0.05 mol $MnFe_2O_4$ (Fig. 9a). The above differences might be due to the effect of the small particle size. Bulk $MnFe_2O_4$ has a spinel-type collinear ferrimagnetic spin structure. Noncollinear spin arrangement at or near the surface of the particleis more pronounced in small particle sizes, which significantly affect the magnetic properties. The cation disorder and magnetically disordered surface layer around the particles could also be responsible for the lower saturation magnetization. Besides, the presence of amorphous impurities (e.g., carbon residue) can also reduce the total magnetization. These MnCA magnetic materials reach the saturation magnetization at relatively low applied fields (ca. 5 kOe). Magnetic Responsiveness of MnCA-0.05is shown in Fig. 10, which displays the MnCA was easy to drive by external magnetic field. The results show MnCAs could be used in other applications, e.g., magnatic resonance imaging, magnetic separation, drug delivery, etc., where need a

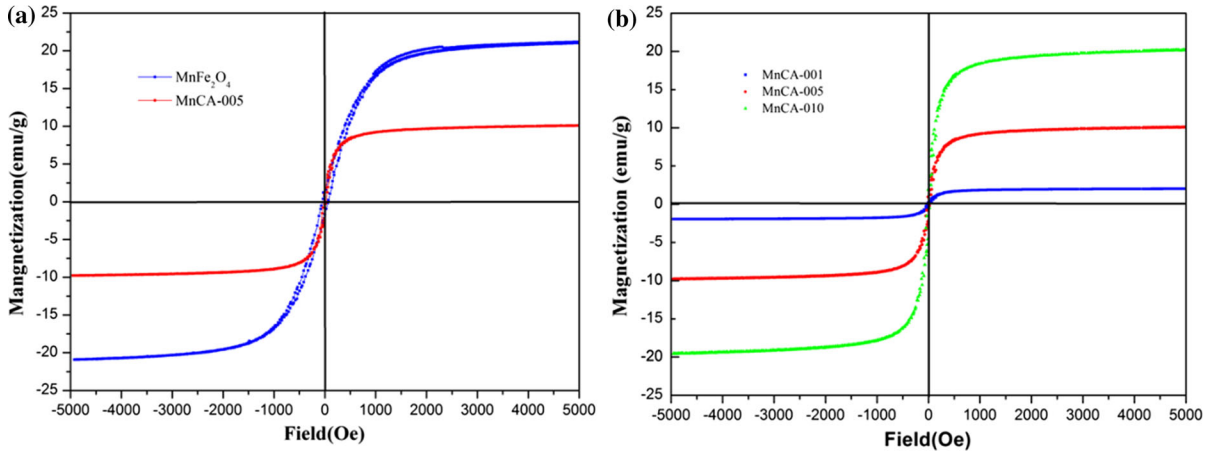

Fig. 9 Hysteresis cycles of $MnFe_2O_4$ and magnetic cellulose aerogels, **a** $MnFe_2O_4$ and MnCA-005, **b** MnCA-001, MnCA-005 and MnCA-010

stong magnetic signal appearing at small applied magnetic fields.

Adsorption property of mangnetic $MnFe_2O_4$-cellulose aerogel towards Cu(II)

Adsorption equilibrium time and adsorption kinetics

The adsorption equilibrium times is an important indicator of the performance of the adsorbent, which directly affects the adsorption efficiency of the adsorbent. Therefore, the effect of adsorption time on the adsorption efficiency offour adsorbents is studied. The oscillating time was 5, 10, 25, 50, 80, 100 and 120 min, respectively. The oscillating time was 50 min, The adsorption rate of the four adsorbents is shown in Fig. 11 after different adsorption times. From the adsorption curve and the adsorption efficiency, it can be seen that the four adsorbents show a very high adsorption efficiency for Cu^{2+} at the initial stage of the adsorption reaction. As time goes on, the adsorption process becomes slow until the final Adsorption balance. This is because at the initial stage of adsorption, there is a concentration difference between the Cu^{2+} and the adsorbed material in the solution to initiate the concentration diffusion, and the active adsorption sites present on the magnetic cellulose are capable of binding to the copper ions, and the adsorption rate and the adsorption amount. But the adsorption activity on the adsorbent is gradually occupied by copper ions, and the concentration gradient of the two is gradually reduced with the progress of the reaction, resulting in the slowing of the adsorption rate until the adsorbent on the adsorption site is completely occupied, the adsorption reaction to reach equilibrium. From the relationship between adsorption time and adsorption efficiency, it can be seen that the adsorption efficiency of MnCA-100 to Cu (II) is close to that of MnCA-005, MnCA-001 and PCA under the same experimental conditions, While

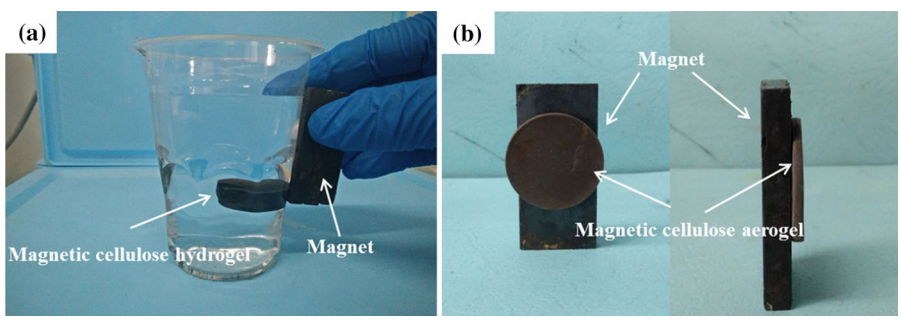

Fig. 10 Macroscopic phenomena of magnetic responsiveness of **a** magnetic cellulose hydrogel, **b** magnetic cellulose aerogel

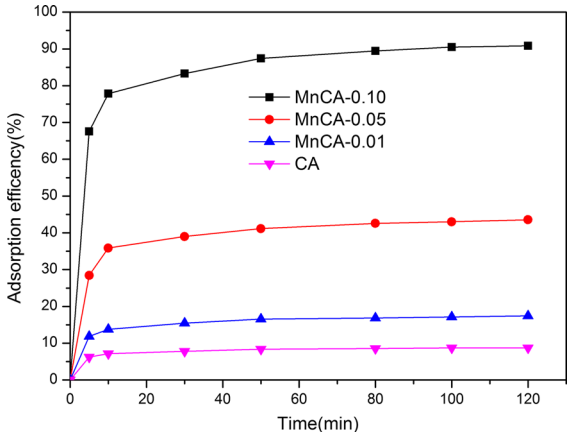

Fig. 11 Adsorption efficiency of CA and MnCA for Cu(II) in different time

the adsorption efficiency of MnCA-005 was 40.1%, the adsorption efficiency of MnCA-001 was 14.8%, while that of pure cellulose aerogels (CA) was only 6.8%, indicating that MnCA-010 has a very strong adsorption capacity for Cu (II) ions.

In order to study the adsorption kinetics of Cu(II) on CA and MnCA, the adsorption data were fitted with pseudo-first-order model (Eq. 5) and pseudo-second-order model (Eq. 6) as follow:

$$\lg(Q_e - Q_t) = \lg Q_e - \frac{k_1 t}{2.303} \quad (5)$$

$$\frac{t}{Q_t} = \frac{t}{Q_e} + \frac{1}{k_2 Q_e^2} \quad (6)$$

where Q_e and Q_t are the adsorption capacity (mg/g) of Cu(II) ions of CA and MnCA at equilibrium and at a given time t respectively, k_1 and k_2 are pseudo-first-order and pseudo-second-order rate constant, respectively.

The parameters of the two models are summarized in Table 2. Though both correlation coefficients R^2 of the two models were greater than 0.9, while the pseudo-second-order kinetic equation provided better correlation of the adsorption process. This indicated that the adsorption process may be mainly controlled by chemisorption. It is obvious that with the increase of $MnFe_2O_4$ content in the magnetic cellulose aerogels, the secondary adsorption rate constant in the quasi-second order kinetic model also increases, indicating that the high $MnFe_2O_4$ content helps to increase the adsorption rate of copper ions. According to the quasi-second order kinetic equation model, the quasi-second rate equation of cellulose aerogels and magnetic cellulose aerogels is plotted with t/Q_t as the ordinate at time t as the abscissa, as shown in Fig. 12. According to fitted curves of CA, MnCA-0.01, MnCA-0.05 and MnCA-0.10, the corresponding correlation coefficients (R^2) were calculated. The R^2 for CA, MnCA-0.01, MnCA-0.05 and MnCA-0.10 are 0.996, 0.995,0996 and 0.998, respectively, indicating that the adsorption of Cu(II) follows the pseudo-second-order kinetic model. The K_2 values are 5.38×10^{-2}, 2.37×10^{-2}, 9.75×10^{-3} and 6.49×10^{-3} g mg^{-1} min^{-1} for MnCA-0.10, MnCA-0.05, MnCA-0.01 and CA, respectively. Apparently, the K_2 values increase with increase of $MnFe_2O_4$ contents. The higher $MnFe_2O_4$ proportion could contribute to the improved adsorption ability of Cu(II).

Adsorption isotherms

In order to further clarify the adsorption thermodynamic mechanism of cellulose aerogel and magnetic cellulose aerogels, the effects of different initial concentrations of Cu(II) on the adsorption properties of Cu^{2+} were studied. In this experiment, 50 mg of adsorbent was added to 50 ml of different initial concentration of Cu^{2+} solution, with range from 10 to 100 mg/L. The pH was adjusted to 6 with dilute hydrochloric acid solution and equilibrated to equilibrium at 25 °C and an oscillation rate of 200 r/min. It can be seen from Fig. 13 that the equilibrium adsorption capacity of the four adsorbents on copper ions increases with the initial concentration of Cu(II) solution until the adsorption is complete. When the Cu(II) solution is at a low concentration, the adsorption curve increases very fast, and when the initial concentration increases to a certain concentration, the rate of increase of the adsorption capacity of the adsorbent gradually begins to slow down, the curve begins to become flat until close Saturated adsorption.

In order to obtain the thermodynamic mechanism of cellulose aerogels and magnetic cellulose aerogels on different initial concentrations of Cu(II) adsorption, Langmuir equation and Freundlich equation were used to fit the experimental data. Langmuir isotherm model (Eq. 7) and Freundlich isotherm model (Eq. 8) as follow:

Table 2 Kinetic parameters of the two kinetic equations for adsorption rate

	Pseudo-first-order equation			Pseudo-second-order equation		
	Q_e	K_1	R_2	Q_e	K_2	R^2
CA	5.866	0.2448	0.9822	6.241	6.49×10^{-3}	0.9998
MnCA-001	11.62	0.2234	0.9807	13.43	9.75×10^{-3}	0.9996
MnCA-005	29.25	0.2161	0.9884	31.13	2.37×10^{-2}	0.9995
MnCA-010	61.48	0.2728	0.9890	64.68	5.38×10^{-2}	0.9996

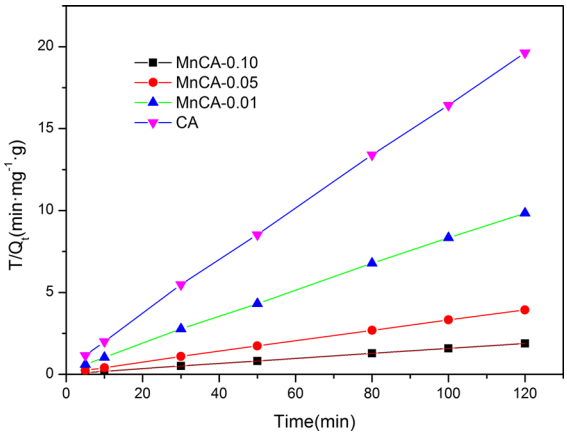

Fig. 12 Pseudo-second-order model for adsorption of Cu(II) on CA, MnCA-001, MnCA-005 and MnCA-010, respectively

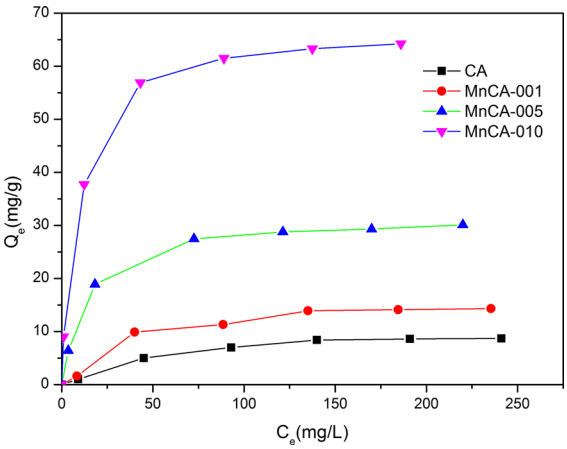

Fig. 13 Adsorption capacity of CA, MnCA-001, MnCA-005 and MnCA-010 for Cu(II) in different initial solution concentration

$$\frac{C_e}{Qe} = \frac{C_e}{Q_m} + \frac{1}{K_L Q_m} \tag{7}$$

$$\ln Q_e = \ln K_F + \frac{1}{n} \ln C_e \tag{8}$$

where Q_e is the absorption capacity of Cu(II) perunit weight of the adsorbent at equilibrium (mg/g) and and Q_m is the maximum adsorption capacity (mg/g), C_e is the adsorption equilibrium concentration of Cu(II) (mg/L), K_L is the Langmuir adsorption equilibrium constant related to the energy, and K_F is related to the adsorption capacity, 1/n is heterogeneity factor.

As shown in Fig. 14, the adsorption data fits the Langmuir model. The correlation coefficients (R^2) for CA, MnCA-0.01, MnCA-0.05 and MnCA-0.10 are 0.9994, 0.9993, 0.9984 and 0.9989, respectively. According to the Langmuir adsorption model, the Q_m of these samples was calculated based on four linear fitting equations. The Q_m is 6.404 mg/g for CA, 13.294 mg/g for 33.036 mg/g and 72.254 mg/g, respectively. Compared with reported Q_m of the iron-oxide based adsorbents, MnCAs exhibited stronger adsorption capacity for Cu(II).

Obviously, the higher content of $MnFe_2O_4$ led to stronger Cu(II) adsorption. The results also reveal that the Cu(II) adsorption capacity was controllable by the contents of $MnFe_2O_4$ in MnCAs. The adsorption capacity of MnCA-010 was much higher than or comparable to those of iron-oxide-based adsorbents. Considering the environmental benefits, the facile convenient preparation method, high specific surface area and strong mechanical strength, easy recycle and separation by magnet attraction, and tunability of Cu(II) adsorption capability, all these properties make the newly synthesized green magnetic cellulose aerogel more favorable and suitable for Cu(II) removal from contaminated water (Table 3).

Fast recycling and reuse of magnetic cellulose aerogels

In the actual water treatment applications, many adsorbents are difficult to recover the problem, especially when the adsorbent on the desorption of

pollutants after removal, it is very difficult to quickly and effectively remove the adsorbent from the water body. In the general small-scale experimental study, the high-speed centrifuge is often used to separate the adsorbent from the wastewater, and the adsorbent is sagged by the action of the centripetal force. The separation effect of this method is obviously effective, but the energy consumption of this method is often Relatively high speed (≥ 2000 r/min) and a longer time to achieve complete separation. And for large-scale water treatment, the centrifugal separation is not applicable, on the one hand is due to disposable centrifugal separation of water sample volume is very limited, the process is cumbersome; Second, requires a lot of driving force, so the magnetic separation technology have a very practical significance. By means of the role of external magnetic field, you can achieve a different magnetic material can be effectively separated. Because the magnetic material in the external magnetic field under the action of the magnetic force is greater than the gravity, with solid–liquid separation efficiency, processing capacity, energy consumption and simple and effective advantages. As shown in Figs. 15a, the magnetic cellulose adsorbent is sufficiently dispersed in the Cu^{2+} ion solution (b), the magnetic cellulose aerogels are attracted by external magnetic fields, and (c) the magnetic cellulose aerogel separates the water samples by magnetic separation. It takes only tens of seconds to achieve rapid separation of the adsorbent

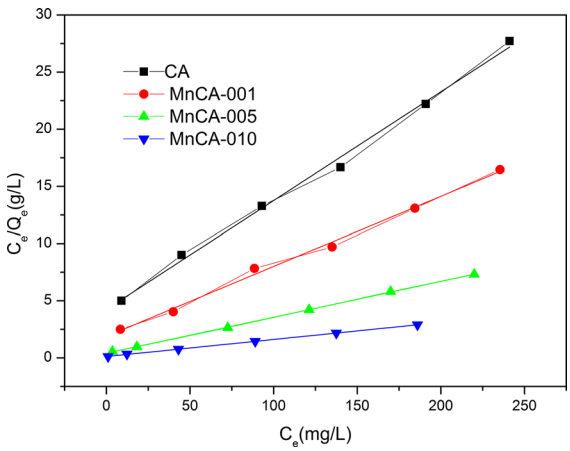

Fig. 14 Langmuir isotherms plots of Cu(II) adsorption on CA, MnCA-001, MnCA-005, MnCA-010, respectively

Table 3 Langmuir and Freundlich parameters for adsorption of Cu(II)

	Langmuir isotherm			Freundich isotherm		
Adsorbent	Q_e(mg/g)	K_L	R^2	K_F	1/n	R^2
CA	10.51	0.0225	0.9950	4.331	0.6138	0.9686
MnCA-001	16.31	0.0327	0.9947	2.876	0.5866	0.9577
MnCA-005	31.84	0.0768	0.9997	1.853	0.6959	0.9218
MnCA-010	67.11	0.1275	0.9997	1.317	0.7293	0.9309

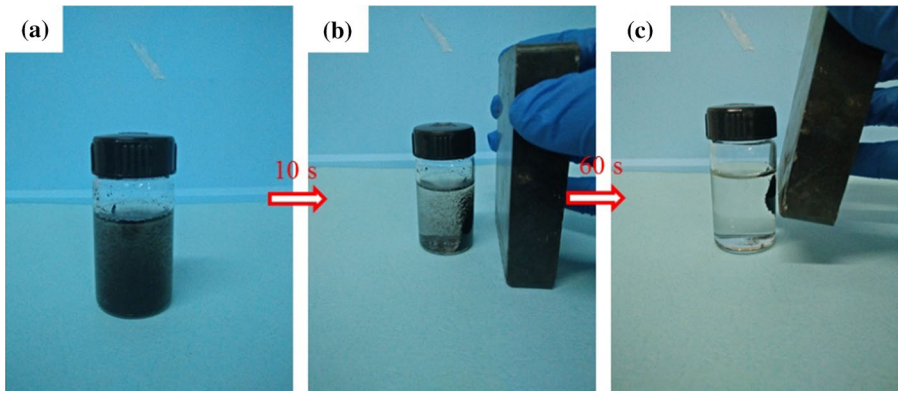

Fig. 15 A simple magnetic separation experiment

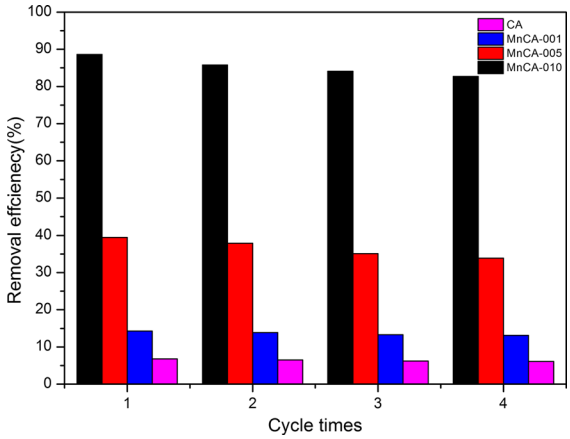

Fig. 16 Cyclic utilization of cellulose aerogel and magnetic cellulose aerogel

and solution, and the effective removal rate is very high.

The regeneration efficiency of the adsorbent is a ten-minute important measure of the practical effect of the adsorbent. In general, the good adsorbent material has a good re-use effect in addition to its high adsorption capacity. The desorption of four adsorbents was also carried out by using 0.2 mol/LEDTA solution as the desorption solution. The results of the repeated use of the four adsorbents were measured. The experimental results are shown in Fig. 16. For the four kinds of adsorption, the removal efficiency of the adsorbent decreased with the increase of the number of adsorbents, but still had better adsorption efficiency. For the magnetic cellulose aerogels MnCA-010, Subcycle of its removal efficiency is still more than 80%. This is due to the EDTA in the desorption process, EDTA heavy metal complexing agent Cu(II) magnetic cellulose aerogels off the surface back to the desorption solution, the adsorbent on the heavy metal adsorption site re-exposure treatment, The adsorbent is thus regenerated, but there are some structural shrinkage and pore clogging in the process of magnetic cellulose aerogels used in the process of desorption and incomplete vacuum desorption.

Adsorption mechanism of MnCA on Cu(II)

In order to study the adsorption mechanism of carboxylated aerated cellulose aerogels on Cu (II), the XPS analysis method was used to determine the presence of elements on the adsorbent surface before and after adsorption of copper ions. Before and after adsorption as show in Fig. 17, The presence of O1 s, C1 s, Fe2p and Mn2p orbits were observed at the binding energies of 531.85, 285.91, 710.88 and 641.41 eV, respectively, before and after adsorption. And a new characteristic peak appeared at 935.2 eV after Cu(II) adsorption, corresponding to the presence of Cu2p orbital (Ren et al. 2012a).

In order to further study the mechanism, Cu2p, O1 s, Fe2p and Mn2p corresponding to the adsorbents adsorbed on Cu(II) were subjected to peak treatment, as shown in Fig. 18c, d, e. Among them, the scanning characteristic peaks corresponding to O1 s can be divided into 3 peaks, corresponding to O1 s in the three different forms of the adsorbent, respectively, at 530.52 eV, the metal oxide (Fe–O or Mn–O), 531.24 eV represents the hydroxyl-bound oxygen

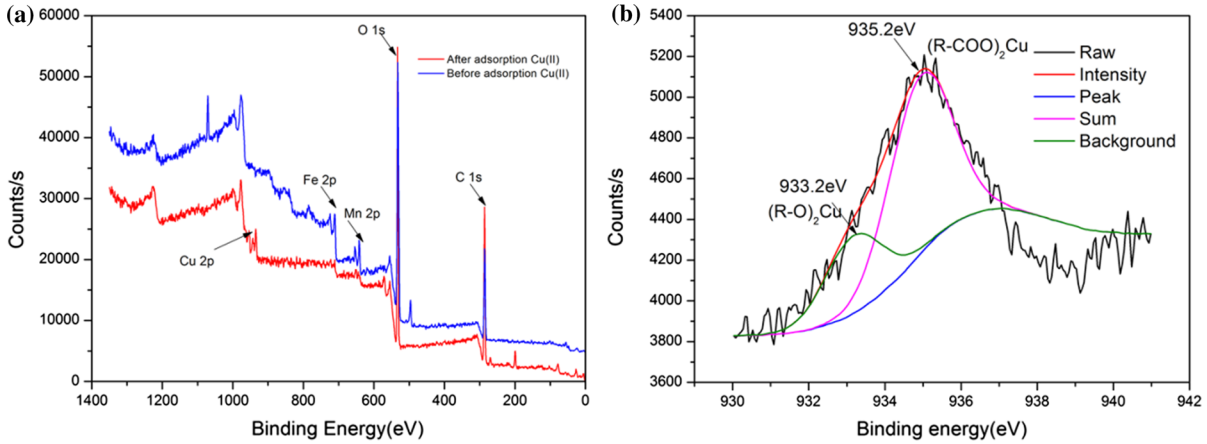

Fig. 17 XPS spectrum of adsorption Cu(II) before and after adsorption by adsorbent, **b** XPS spectrum of Cu2p after peak-fit processing

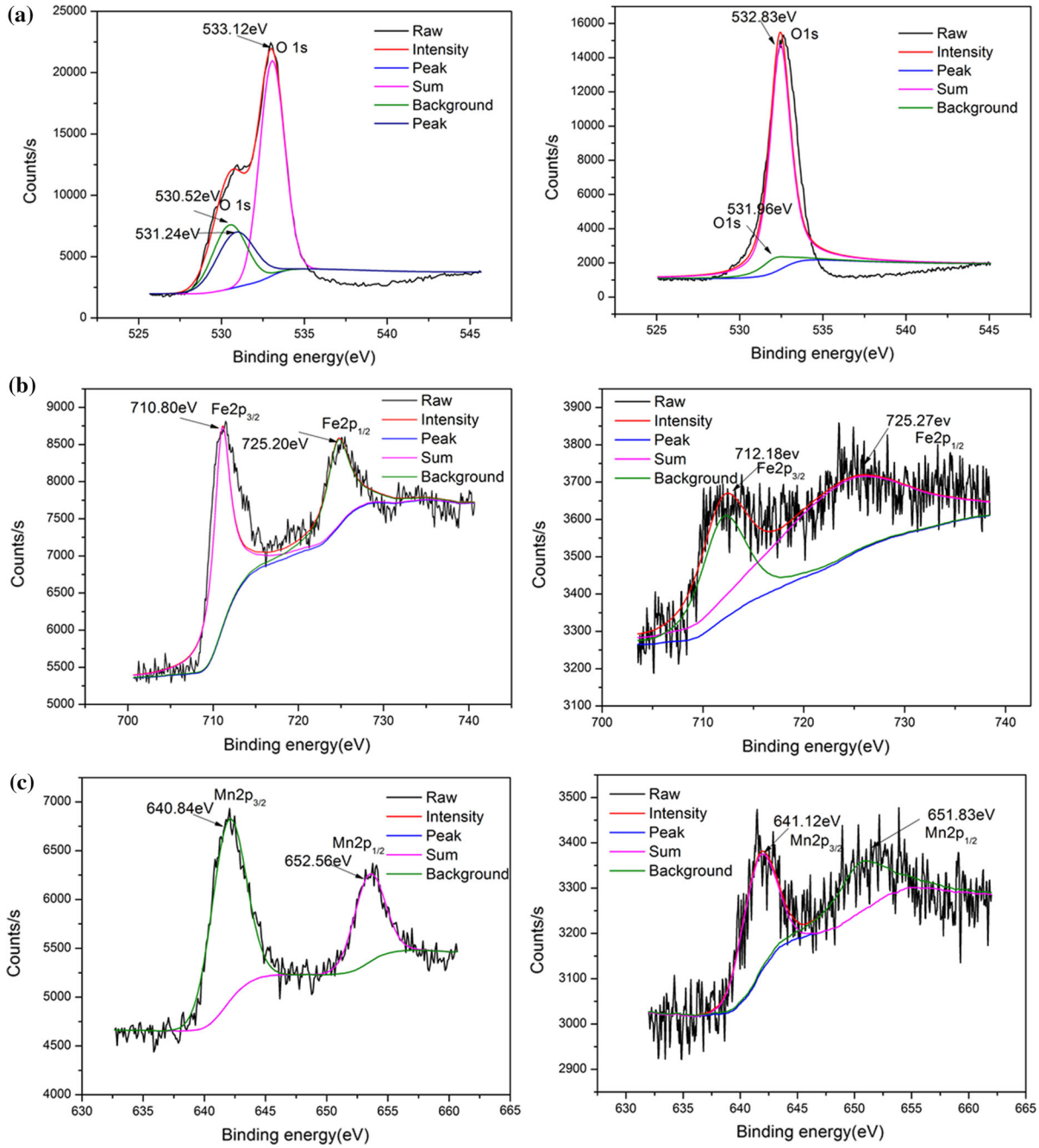

Fig. 18 XPS spectrums after peak-fit processing of adsorption Cu(II) before and after adsorption, **a** O 1 s, **b** Fe2p, **c** Mn2p

(−OH), and 533.12 eV represents the presence of (-COOH) (Ren et al. 2012a). The peak area of O1 s before adsorption was significantly smaller than that of O1 s before adsorption, and the peak at 531 eV was not obvious, showing a trend toward the middle, indicating that the hydroxyl and carboxyl functional groups possessed by the adsorbent cut back. And the peak area of metal oxidation also changed to a certain extent, combined with Fig. 18b, it should be Cu(II) and adsorbent reaction combined with part of the O1 s, oxygen-containing functional groups involved in the adsorption process, The peak area of Cu2p is probably

the position of copper to replace the original hydrogen ion, forming the corresponding complex. Fe2p and Mn2p have a very positive effect on the adsorption of Cu(II) in the direction of high binding energy, while Mn2p is shifted toward the low binding energy, and $MnFe_2O_4$ with a very positive effect on the adsorption of Cu(II), Fe–O bond and Mn–O bond are involved in the copper ion adsorption reaction.

Conclusions

$MnFe_2O_4$-Cellulose magnetic composite aerogels (MnCAs) with high adsorption capacity for metal ions were fabricated by in situ incorporation of $MnFe_2O_4$ in the cellulose hydrogel matrix. The surface area, pore characteristic parameters and magnetic property of the synthesized $MnFe_2O_4$ could be tailored by adjusting the total concentrations of the $FeCl_3/MnCl_2$ salts. The magnetic cellulose aerogels exhibited superior magnetic responsiveness and can be easily actuated by an applied magnetic field. Moreover, the MnCA nanocomposites also displayed rapid removal efficiency and excellent adsorption ability to remove Cu(II) ions, and easy recycle and separation by magnet attraction. Hence, the green magnetic cellulose aerogel could be expected to be a new adsorbent material for removal heavy metal ions from water effluent.

Acknowledgment This work was financially supported by the NSFC (81471183), the clinical medical special Program of Science and Technology Project of Jiangsu Province (BL2014074), the Industry Program of Science and Technology Support Project of Jiangsu Province (BE2014128, BE2016171), the Prospective Joint Research Program of Jiangsu Province (BY2015005-01), the Major Program of Natural Science Fund in Colleges and Universities of Jiangsu Province (15KJA430005), the General Program of Social Development Project of Jiangsu Province (BE2015672), the Program for Changjiang Scholars and Innovative Research Team in University (No.IRT_15R35) and the Priority Academic Program Development of Jiangsu Higher Education Institutions (BK2014377). Any opinions, findings, and conclusions or recommendations expressed in this paper are those of the authors and do not necessarily reflect the views of these programs.

References

Abramian L, El-Rassy H (2009) Adsorption kinetics and thermodynamics of azo-dye Orange II onto highly porous titania aerogel. Chem Eng J 150:403–410. https://doi.org/10.1016/j.cej.2009.01.019

Aslibeiki B et al (2016) Solvothermal synthesis of $MnFe_2O_4$ nanoparticles: the role of polymer coating on morphology and magnetic properties. J Magn Magn Mater 399:236–244. https://doi.org/10.1016/j.jmmm.2015.09.081

Baccar R, Bouzid J, Feki M, Montiel A (2009) Preparation of activated carbon from Tunisian olive-waste cakes and its application for adsorption of heavy metal ions. J Hazard Mater 162:1522–1529. https://doi.org/10.1016/j.jhazmat.2008.06.041

Baetens R, Jelle BP, Gustavsen A (2011) Aerogel insulation for building applications: a state-of-the-art review. Energ Buildings 43:761–769. https://doi.org/10.1016/j.enbuild.2010.12.012

Cai J, Zhang L (2006) Unique gelation behavior of cellulose in NaOH/Urea aqueous solution. Biomacromol 7:183–189. https://doi.org/10.1021/bm0505585

Cai J, Kimura S, Wada M, Kuga S, Zhang L (2008) Cellulose aerogels from aqueous alkali hydroxide-urea solution. Chemsuschem 1:149–154. https://doi.org/10.1002/cssc.200700039

Cai J, Liu S, Feng J, Kimura S, Wada M, Kuga S, Zhang L (2012) Cellulose-Silica Nanocomposite Aerogels by In Situ Formation of Silica in Cellulose Gel. Angew Chem Int Ed 51:2076–2079. https://doi.org/10.1002/anie.201105730

Cui S, Cheng W, Shen X, Fan M, Russell A, Wu Z, Yi X (2011) Mesoporous amine-modified SiO_2 aerogel: a potential CO_2 sorbent. Energ Environ Sci 4:2070–2074. https://doi.org/10.1039/c0ee00442a

Dassanayake RS, Gunathilake C, Jackson T, Jaroniec M, Abidi N (2016) Preparation and adsorption properties of aerocellulose-derived activated carbon monoliths. Cellulose 23:1363–1374. https://doi.org/10.1007/s10570-016-0886-1

Dou B, Li J, Wang Y, Wang H, Ma C, Hao Z (2011) Adsorption and desorption performance of benzene over hierarchically structured carbon-silica aerogel composites. J Hazard Mater 196:194–200. https://doi.org/10.1016/j.jhazmat.2011.09.019

Fu F, Wang Q (2011) Removal of heavy metal ions from wastewaters: a review. J Environ Manage 92:407–418. https://doi.org/10.1016/j.jenvman.2010.11.011

Jusoh A, Shiung LS, Na Ali, Noor MJMM (2007) A simulation study of the removal efficiency of granular activated carbon on cadmium and lead. Desalination 206:9–16. https://doi.org/10.1016/j.desal.2006.04.048

Kang KC, Kim SS, Choi JW, Kwon SH (2008) Sorption of Cu^{2+} and Cd^{2+} onto acid- and base-pretreated granular activated carbon and activated carbon fiber samples. J Ind Eng Chem 14:131–135. https://doi.org/10.1016/j.jiec.2007.08.007

Kefeni KK, Mamba BB, Msagati TAM (2017) Application of spinel ferrite nanoparticles in water and wastewater treatment: a review. Sep Purif Technol 188:399–422. https://doi.org/10.1016/j.seppur.2017.07.015

Lin BL, Cui S, Liu XY, Liu Y, Shen XD, Han GF (2013) Preparation and adsorption property of phenyltriethoxysilane modified SiO_2 aerogel. J WuHan Univ Technol-Mat

Sci Edit 28:916–920. https://doi.org/10.1007/s11595-013-0793-3

Liu P, Long C, Li QF, Qian HM, Li AM, Zhang QX (2009) Adsorption of trichloroethylene and benzene vapors onto hypercrosslinked polymeric resin. J Hazard Mater 166:46–51. https://doi.org/10.1016/j.jhazmat.2008.10.124

Liu S, Zhou J, Zhang L (2011) In situ synthesis of plate-like Fe_2O_3 nanoparticles in porous cellulose films with obvious magnetic anisotropy. Cellulose 18:663–673. https://doi.org/10.1007/s10570-011-9513-3

Liu S, Tao D, Zhang L (2012a) Cellulose scaffold: a green template for the controlling synthesis of magnetic inorganic nanoparticles. Powder Technol 217:502–509. https://doi.org/10.1016/j.powtec.2011.11.010

Liu S, Yan Q, Tao D, Yu T, Liu X (2012b) Highly flexible magnetic composite aerogels prepared by using cellulose nanofibril networks as templates. CarbohydPolym 89:551–557. https://doi.org/10.1016/j.carbpol.2012.03.046

Liu G et al (2014) An ecological risk assessment of heavy metal pollution of the agricultural ecosystem near a lead-acid battery factory. Ecol Indic 47:210–218. https://doi.org/10.1016/j.ecolind.2014.04.040

Maleki H (2016) Recent advances in aerogels for environmental remediation applications: a review. Biochem Eng J 300:98–118. https://doi.org/10.1016/j.cej.2016.04.098

Mi X, Huang GB, Xie WS, Wang W, Liu Y, Gao JP (2012) Preparation of graphene oxide aerogel and its adsorption for Cu^{2+} ions. Carbon 50:4856–4864. https://doi.org/10.1016/j.carbon.2012.06.013

Monser L, Adhoum N (2002) Modified activated carbon for the removal of copper, zinc, chromium and cyanide from wastewater. Sep Purif Technol 26:137–146. https://doi.org/10.1016/S1383-5866(01)00155-1

Mu R-J, Pang J, Yuan Y, Tan X-D, Wang M, Chen H, Wei-Yin C (2016) Progress on the Structures and Functions of Aerogels. Chinese J Struc Chem 35:487–497. https://doi.org/10.14102/j.cnki.0254-5861.2011-1098

Naushad M, Ahamad T, Al-Maswari BM, Alqadami AA, Alshehri SM (2017) Nickel ferrite bearing nitrogen-doped mesoporous carbon as efficient adsorbent for the removal of highly toxic metal ion from aqueous medium. Chem Eng J 330:1351–1360. https://doi.org/10.1016/j.cej.2017.08.079

Olsson RT et al (2010) Making flexible magnetic aerogels and stiff magnetic nanopaper using cellulose nanofibrils as templates. Nat Nanotechnol 5:584–588. https://doi.org/10.1038/nnano.2010.155

Pizarro J et al (2015) Adsorption of Cu^{2+} on coal fly ash modified with functionalized mesoporous silica. Fuel 156:96–102. https://doi.org/10.1016/j.fuel.2015.04.030

Qarri F, Lazo P, Bekteshi L, Stafilov T, Frontasyeva M, Harmens H (2015) The effect of sampling scheme in the survey of atmospheric deposition of heavy metals in Albania by using moss biomonitoring. Enviro Sci Pollut R 22:2258–2271. https://doi.org/10.1007/s11356-014-3417-3

Rajput S, Pittman CU, Mohan D (2016) Magnetic magnetite (Fe_3O_4) nanoparticle synthesis and applications for lead (Pb^{2+}) and chromium (Cr^{6+}) removal from water. J Colloid Interf Sci 468:334–346. https://doi.org/10.1016/j.jcis.2015.12.008

Ren Y, Li N, Feng J, Luan T, Wen Q, Li Z, Zhang M (2012) Adsorption of Pb(II) and Cu(II) from aqueous solution on magnetic porous ferrospinel $MnFe_2O_4$. J Colloid Interf Sci 367:415–421. https://doi.org/10.1016/j.jcis.2011.10.022

Shen C, Chen C, Wen T, Zhao Z, Wang X, Xu A (2015) Superior adsorption capacity of g-C_3N_4 for heavy metal ions from aqueous solutions. J Colloid Interf Sci 456:7–14. https://doi.org/10.1016/j.jcis.2015.06.004

Shim WG, Lee JW, Moon H (2006) Adsorption equilibrium and column dynamics of VOCs on MCM-48 depending on pelletizing pressure. Micropor Mesopor Mat 88:112–125. https://doi.org/10.1016/j.micromeso.2005.08.026

Standeker S, Novak Z, Knez Z (2007) Adsorption of toxic organic compounds from water with hydrophobic silica aerogels. J Colloid Interf Sci 310:362–368. https://doi.org/10.1016/j.jcis.2007.02.021

Stergar J, Maver U (2016) Review of aerogel-based materials in biomedical applications. J Sol-Gel Sci Techn 77:738–752. https://doi.org/10.1007/s10971-016-3968-5

Vernekar AA, Das T, Ghosh S, Mugesh G (2015) A remarkably efficient $MnFe_2O_4$-based oxidase nanozyme. Chem Asian J 11:72–76. https://doi.org/10.1002/asia.201500942

Wang Z, Liu S, Matsumoto Y, Kuga S (2012) Cellulose gel and aerogel from LiCl/DMSO solution. Cellulose 19:393–399. https://doi.org/10.1007/s10570-012-9651-2

Wang Y, Wu X, Zhang W, Huang S (2016) Synthesis and electromagnetic absorption properties of Ag-coated reduced graphene oxide with $MnFe_2O_4$ particles. J Magn Magn Mate 404:58–63. https://doi.org/10.1016/j.jmmm.2015.12.028

Wu Q, Cui Y, Li Q, Sun J (2015) Effective removal of heavy metals from industrial sludge with the aid of a biodegradable chelating ligand GLDA. J Hazard Mater 283:748–754. https://doi.org/10.1016/j.jhazmat.2014.10.027

Zeng H, Rice PM, Wang SX, Sun S (2004) Shape-controlled synthesis and shape-induced texture of $MnFe_2O_4$ nanoparticles. J Am Chem Soc 126:11458. https://doi.org/10.1021/ja045911d

Zeng L et al (2015) Adsorption of Cd(II), Cu(II) and Ni(II) ions by cross-linking chitosan/rectorite nano-hybrid composite microspheres. Carbohyd Polym 130:333–343. https://doi.org/10.1016/j.carbpol.2015.05.015